TRI-PP-85-20
Apr 1985

Study of the ^{3}He(p,2p)d and ^{3}He(p,pd)p Reactions at Large Recoil Momenta*

M. B. Epstein, D. A. Krause, and D. J. Margaziotis
Department of Physics and Astronomy
California State University, Los Angeles, CA 90032, USA
and
A. Bracco+, H. P. Gubler++, D. K. Hasell+++, and W. P. Lee++++
Department of Physics
University of Manitoba, Winnipeg, Manitoba R3T 2N2, Canada
and
W. T. H. van Oers
TRIUMF, Vancouver B.C. V6T 2A3, Canada, and
Department of Physics
University of Manitoba, Winnipeg, Manitoba R3T 2N2, Canada
and
R. Abegg, and C. A. Miller
TRIUMF, Vancouver B.C. V6T 2A3, Canada, and
Nuclear Research Center
University of Alberta, Edmonton, Alberta, T6G 2J1, Canada
and
A. W. Stetz
Department of Physics
Oregon State University, Corvallis, OR 97331, USA

(Submitted to Physical Review C)

ABSTRACT

Quasi-free p-p and p-d scattering from ^{3}He at intermediate energies have been studied. The ^{3}He(p,2p)d reaction has been measured at 300 MeV at the angle pair 70^o-33^o and at 450 MeV at the angle pairs 70^o-30^o and 46^o-46^o for recoil momenta between 350 and 530 MeV/c. For the ^{3}He(p,pd)p reaction, energy sharing loci have been measured at 300 MeV at the angle pair 70^o-33^o and at 450 MeV for the angle pairs 25^o-68^o, 50^o-68^o, and 70^o-30^o yielding a recoil momentum range from 0 to 480 MeV/c. The spectral function S(E,q) with E equal to the two-body breakup energy for ^{3}He has been deduced from the present results in the framework of the PWIA as a function of the p-d relative momentum q. The spectral function is compared with other spectral functions obtained from previous ^{3}He(p,pd)p and ^{3}He(e,e'p)d experiments and with existing theoretical predictions.

Nuclear reactions ^{3}He(p,2p)d and ^{3}He(p,pd)p; measured $d^5\sigma/d\Omega_3 d\Omega_4 dT_3$ at 300 and 450 MeV; deduced spectral function in PWIA; comparison with theoretical predictions.

PACS 20.25

INTRODUCTION

Studies of intermediate energy knock-out reactions provide information relevant to both nuclear structure and the reaction mechanism. It is well known that to extract nuclear wave function information one should be able to calculate the off-energy-shell effective t matrix, and make corrections for final state interactions, multistep processes, and three body effects but one expects that in the case of the very light nuclei such as ^{2}H, ^{3}He, ^{3}H, and ^{4}He some of these effects are minimized. In particular the (p,2p), (p,pd), (e,e'p) and (e,e'd) reactions on ^{3}He should provide significant insight into the wavefunction of the three-nucleon system. At present, many properties of the three-nucleon nuclei are not yet understood and the comparison between experimental data and theoretical predictions is an important tool in understanding the limitations of the classic non-relativistic three-nucleon wavefunction. The classical description of the three-nucleon system does not account for mesonic and internal nucleonic quark degrees of freedom; the task of including them is extremely difficult and results will not be immediate.

The primary objective of the present measurements of the $^{3}He(p,2p)d$ and $^{3}He(p,pd)p$ reactions is to provide additional and new information useful to the understanding of the three-nucleon system. Differential cross sections were measured over a large range of recoil momenta including a large recoil region (up to 530 meV/c), previously unexplored. The investigation of the high

recoil momentum region of the proton-deuteron relative motion momentum distribution is particularly interesting because it corresponds to short distances of the wavefunction in configuration space. Furthermore, the comparison of the two reactions allows one to learn more about the reaction mechanism and it provides a test for the Plane Wave Impulse Approximation (PWIA) assumptions.

In the framework of the Impulse Approximation, an incident proton interacts strongly only with the ejected proton (in the p,2p reaction) or deuteron (in the p,pd reaction) while the recoiling nucleus acts as spectator. These reactions are described by the first-order diagrams of Fig. 1. In the PWIA the motion of the center of mass of the reaction participants in the initial and final states is described by plane waves.

Quantitatively, the PWIA differential cross section of either of these two reactions factors into the following terms:

$$\frac{d^5\sigma}{d\Omega_3 d\Omega_4 dT_3} = F\left(\frac{d\sigma}{d\Omega}\right)^{p-i}\left[N|\phi(q)|^2\right] \qquad (1)$$

where F is the three-body phase space factor involving known kinematic quantities, $(d\sigma/d\Omega)^{p-i}$ is the half-off-energy-shell p-p or p-d differential cross section and $\phi(q)$ is the Fourier transform of the overlap integral between the ^{3}He and deuteron wave functions with q being the p-d relative momentum in the target nucleus which is equal to the recoil momentum of the unobserved (spectator) particle.

$$\phi(\bar{q}) = \frac{1}{(2\pi)^{3/2}}\int e^{i\bar{q}\cdot\bar{r}} \langle \psi_d | \psi_{^3He} \rangle d\bar{r} \qquad (2)$$

N is a spectroscopic factor determined from spin algebra (N = 3/2 for the reaction considered here). The quantity $|\phi(q)|^2$ describes the p-d relative motion momentum density distribution in ^{3}He. The product $N|\phi(q)|^2$ is equivalent to the spectral function S(q,E), i.e. the joint probability of finding a proton in the target nucleus with momentum q and separation energy E leading to the p-d final state. Commonly, the half-off-energy-shell differential cross section is replaced by the on-energy-shell differential cross section for free p-p or p-d scattering. It is noted that, since the lower vertex in the two diagrams of Fig. 1 is the same, the momentum distribution extracted from the (p,2p) and (p,pd) reactions should be the same. Also $|\phi(q)|^2$ can be unambigously determined in the PWIA only when the energy of the scattered and ejected particles is much larger than the energy of the recoil system.

This simple description of the two knockout processes neglects many effects such as multiple scattering, final state interactions, and isobar configurations but still accounts for the dominant part of the reaction and at least at low q is particularly meaningful as a first step of the investigation. In addition, only in the framework of the PWIA it is possible to compare directly the theoretical spectral function with the experimental momentum distributions as extracted from the ^{3}He(p,2p)d, ^{3}He(p,pd)p, ^{3}He(e,e´p)d, and ^{3}He(e,e´d)p reactions.

The ^{3}He (p,2p)d and ^{3}He(p,pd)p reactions were previously

measured at 35, 45, 65, 85 and 100 MeV (Ref. 1) sampling recoil momenta less than 130 MeV/c. At higher energies the two reactions were measured at 155 MeV (Ref. 2) and 590 MeV (Ref. 3). The momentum distributions extracted from the ^{3}He(p,2p)d and ^{3}He(p,pd)p reactions at 155 MeV cover a range between 0 and 120 MeV/c and are in good agreement with each other indicating the validity of the factorization for the five-fold differential cross section in the PWIA. The ^{3}He(p,2p)d data obtained at 590 MeV could not be directly compared with the ^{3}He(p,pd)p data at the same incident energy because the data lacked adequate resolution so that a separation between ^{3}He(p,2p)d and ^{3}He(p,2p)d* was not possible. For the ^{3}He(p,pd)p reaction at 590 MeV, recoil momenta up to 230 MeV/c were obtained. The present study of the ^{3}He(p,2p)d and ^{3}He(p,pd)p reactions has been reported in part, in a previous letter (Ref. 4). Here a more complete and detailed description of the experiment is given. The experimentally derived spectral function will be compared to theoretical predictions calculated for different nucleon-nucleon potentials based on Faddeev or variational techniques.

EXPERIMENTAL PROCEDURE

The experiment was performed using the proton beam from the variable energy TRIUMF accelerator incident on a liquid ^{3}He target (Ref. 5). Beam intensities ranged between 0.5 nA and 5 nA. The beam position and direction were measured using wire profile monitors and by viewing a fluorescent screen which could

be placed at the target position. The cross section of the beam at the target was about 0.5 cm in diameter. Normalization of the differential cross sections was obtained from the sum of the left and right counts of the incident beam polarimeter (containing a 5 mg/cm^2 thick CH_2 target) located upstream of the L^3He target. The incident beam polarimeter had been previously calibrated against a Faraday cup. The target thickness followed from measurements of the L^3He temperature in the target cell through germanium resistors embedded in the body of the cell and from its physical dimensions. The thickness so determined was 104 ± 4 mg/cm^2 ^3He. The target cell radius was 2.2 cm. The target cell could be raised or lowered remotely. This permitted the L^3He target cell to be replaced with either an identical dummy cell in order to allow appropriate background subtractions or by a fluorescent screen. The target cell could also be rotated around a central vertical axis in order to ensure that the reaction products would not strike the sides of the cell frame.

The $^3He(p,2p)d$ reaction was measured at 300 MeV at the angle pair 70^o-33^o and at 450 MeV at the angle pairs 70^o-30^o and 46^o-46^o ; it was used to explore the recoil momentum range between 300-530 MeV/c. The combined energy resolution of the incident beam and the detection apparatus was not quite adequate to resolve the $^3He(p,2p)d$ locus from the four body continuum when detecting only two protons. Therefore, the recoil deuteron was detected in a triple coincidence arrangement together with the scattered and ejected protons. As a consequence, the range of recoil momenta accessible through the (p,2p) reaction was

restricted to q > 300 MeV/c corresponding to the minimum detectable energy for the deuteron. The momentum of the ejected proton was measured by a magnetic spectrometer (MRS) placed on the large-angle side of the incident beam while two identical NaI(Tl) counter telescopes were used to detect the scattered proton and the recoil deuteron on the right-hand side with respect to the incident beam direction.

The counter telescopes were mounted on a platform and were positioned with an accurace of $\pm0.1^o$. Each counter telescope consisted of a 12.8 cm by 12.8 cm delay-line multiwire proportional chamber (DLC) with 0.2 cm wire spacing followed immediately by a thin ΔE plastic scintillator (0.08 cm thick), an annular veto counter (with an aperture of 10.2 cm in diameter), and a 12.7 cm diameter by 15.2 cm thick NaI(Tl) detector preceded by copper degrader when required. The MRS detection system consisted of a quadrupole-dipole magnet combination. Upstream of this combination, a 0.08 cm thick plastic scintillator was used to provide a timing signal and a 12.8 cm by 12.8 cm multiwire proportional counter (MWPC) (with 0.2 cm wire spacing) was used to define the solid angle. The dipole magnet was followed by a set of 25.6 cm by 102.4 cm MWPC's (with 0.2 cm wire spacing), mounted about the focal plane of the spectrometer, and by a 2.5 cm thick plastic scintillator. The time-of-flight path through the spectrometer was ~11.0 m. Events were recorded for a double coincidence between the thin plastic scintillator of the counter telescope detecting the scattered proton and the plastic scintillator at the entrance of the spectrometer with no signal

present in the veto counter. Through software, a triple coincidence could be imposed off-line to account for the simultaneous detection of the recoil deuteron in the second counter telescope.

The region of lower recoil momenta (5-450 MeV/c) was explored through the ^{3}He(p,pd)p reaction. This reaction was measured at an incident energy of 450 MeV at the angle pairs 25^o-68^o and 50^o-68^o. At the first angle pair a complete energy spectrum was measured corresponding to recoil momenta from 0 to 450 MeV/c, while at the second pair only part of the energy spectrum was measured. The kinematical conditions chosen correspond to large relative energies between the three final state particles and a small momentum transfer $|\vec{p}_1-\vec{p}_3|$ ($\vec{p}_1$ and $\vec{p}_3$ are the momenta of the particles as shown in Fig 1). The first requirement reduces the final state interactions between the reaction products, the second assures a larger p-d differential cross section which is necessary to maintain an adequate counting rate at large recoil momenta. The momentum of the ejected deuteron was measured with the MRS placed on the large-angle side of the incident beam, while the energy of the scattered proton was measured by either one of the two right-hand-side counter telescopes. Due to the limited deuteron momentum bite in the spectrometer, the energy sharing spectra were measured in a series of overlapping energy bites achieved by changing the magnetic field values of the quadrupole and dipole magnets. A limited amount of ^{3}He(p,pd)p data was also obtained simultaneously with the ^{3}He(p,2p)d data at 300 MeV (70^o-33^o) and

at 450 MeV(70^o-30^o) where the scattered proton was detected by the MRS and the deuteron was detected by the counter telescope used for the ejected proton of the (p,2p) events. These data cover the recoil momentum range between 80-290 MeV/c.

The energy calibration of the counter telescopes was obtained by observing proton-proton scattering from a CH_2 target at a series of angles covering the range of energies of interest. For each ^{3}He(p,2p)d and ^{3}He(p,pd)p measurement, a separate determination was made of the background by replacing the L^{3}He target cell with the dummy cell.

DATA REDUCTION AND EXPERIMENTAL RESULTS

From all events recorded on tape, only events which satisfied a number of conditions were selected for the computation of the reaction yields. For example, events were rejected when any one of the MWPC planes had a missing wire coordinate or when non-adjacent wires were firing in a single plane with a gap greater than one wire. Events which showed pile-up within an interval of 300 ns in the NaI (Tl) detector signal were also rejected. Solid angles were chosen to correspond to the flat efficiency region of the NaI(Tl) detectors (Ref.6) while insuring that the corresponding kinematically allowed MRS region was within the flat response region of the MRS angular acceptance. Real concidences were subtracted from accidentals using standard techniques. Finally, events were restricted to those belonging to the kinematic locus of the ^{3}He(p,2p)d or ^{3}He(p,pd)p reaction

as identified by an appropriate cut around the peak in the missing energy spectrum. Missing energy is defined as $E_m = T_3+T_4+T_5-T_1$, where the T_i (i = 1,3,4,5) are the laboratory kinetic energies of the particles shown in Fig. 1. A typical missing energy spectrum is shown in Fig. 2. The centroid of the peak has the value of the two-body breakup energy for ^{3}He and its width depends on the combined energy resolution of the NaI(Tl) counter telescopes, magnetic spectrometer and the incident proton beam. The combined resolution varied from 8 to 10 MeV (FWHM) depending on the thickness of the Cu absorber preceding the NaI(Tl) detectors. The energy resolution of the counter telescopes varied between 7 and 9 MeV(FWHM).

The resulting yields were corrected for MWPC inefficiencies due to missing or non-adjacent hits, MRS inefficiency due to events not completing their path through the dipole, NaI(Tl) detector inefficiencies due to nuclear reaction losses (Ref.6), losses due to data acquisition system dead time and losses due to pile-up. The data were also corrected for background events from the entrance and exit foils of the target cell and cryostat tail section by subtracting similarly processed data taken with the dummy (empty) cell. The fivefold differential cross sections were obtained from 10 MeV bites in the kinetic energy T_3 of the scattered particle for the ^{3}He(p,2p)d reaction and from 10 MeV bites in the kinetic energy T_4 of the ejected particle for the ^{3}He(p,pd)p reaction. The results of the measurements of the ^{3}He(p,2p)d reaction are presented in Table 1 and the ones of the ^{3}He(p,pd)p reaction in

Table 2. The errors reported in the tables are statistical only. The uncertainty in the absolute normalization of the differential cross sections is estimated to be $\pm$10%. It includes contributions from the uncertainties in the determination of the total number of incident protons (~ 5%), NaI(Tl) detector efficiency (~1%), MWPC efficiency (~1%), solid angle (~1%), target thickness (from 3% to 4%), and electronics and computer dead time (~1.5%).

The experimental p-d relative motion momentum distribution was extracted from the obtained differential cross sections using the PWIA prescription described by Eqn. 1. The half-off-energy-shell p-p and p-d differential cross sections were approximated by on-energy-shell values. The required differential cross sections were evaluated using the final state approximation i.e. in the center of mass system of the scattered and ejected particles. The corresponding incident proton laboratory energies (T_{lab}) and scattering angles in the center of mass (θ_{cm}) are shown in Tables 1 and 2 for p-p and p-d scattering respectively. The p-p differential cross sections of Table 1 were calculated from phase shift analyses (Ref. 7), while the p-d differential cross sections of Table 2 were obtained from spline fits of existing data (Ref. 8).

The resulting spectral function values $N|\phi(q)|^2$ derived from the present experiment are shown in Fig. 3-6 where they are compared with results from previous (p,pd) and (e,e'p) measurements and with theoretically derived spectral functions.

DISCUSSION

The experimental spectral function extracted from these measurements is shown in Fig. 3 plotted as a function of the relative proton-deuteron momentum q. This figure includes all (p,2p) and (p,pd) results obtained in this experiment. All these data yield self-consistent values for the spectral function except, perhaps, for the "simultaneous" (p,pd) data described previously. This is in spite of the fact that the data have been obtained using two different reactions, different incident energies and under varying kinematic conditions. In view of this, the rather smooth distribution of the resulting spectral function values suggests that the PWIA represents the dominant reaction mechanism operating here. It is perhaps particularly interesting to consider the range of kinematic conditions sampled by the high recoil momentum data, since in this region one would expect other reaction mechanisms to be at least comparable in strength to the PWIA quasifree scattering. The data in this region cover, in addition to the two different incident energies, a fairly wide range of relative energies, T_{ij}, between pairs of particles in the final state. For example for q around 400 MeV/c the four data points shown cover a range of p-d relative energies T_{45} between 11 and 175 MeV and for T_{35} between 163 and 271 MeV. The corresponding relative p-p energies T_{34} range from 63 to 246 MeV. Moreover, since this region includes (p,pd) as well as (p,2p) data both free p-d and p-p differential cross sections had to be used to extract the spectral function. Since final state

interactions and intermediate virtual delta excitation depend strongly on T_{ij}, it may be reasonable to take the scatter in these data about a given recoil momentum as a combined measure of these effects, as well as reflecting the uncertainties in the p-d differential cross sections used in the PWIA. The higher values of some of the "simultaneous" (p,pd) data, especially at the larger recoil momenta q, may indicate the presence of final state interaction effects, as the data were taken under kinematic conditions involving rather low values of T_{45}.

Also shown in the figure are the (p,pd) data obtained at SREL at 590 MeV. These data tend to produce somewhat smaller values than the present data, on the other hand it is not clear that the SREL spectral function values were derived from the measured differential cross sections using quite an equivalent procedure.

The curves shown in Fig. 3 are some of the most recent PWIA predictions for the ^{3}He spectral function calculated using various techniques and different nucleon-nucleon potentials to obtain wave function information from the Schrodinger equation. Curve 1 is the spectral function calculated by Ciofi degli Atti et al. (Ref. 9) using the variational wave function of Nunberg et al. (Ref. 10) with correct asymptotic behavior of the harmonic oscillator basis expansion wave function. Curve 3 is the spectral function calculated by Dieperink et al. (Ref. 11) from the ^{3}He ground state wave function obtained by Brandenburg et al. (Ref. 12) using Faddeev techniques and the Reid soft-core (RSC) potential limited to $^1S_0$ and $^3S_1 - {}^3D_1$ states. Curves 2 and 4

are spectral functions calculated by Meier-Hajduk et al. (Ref. 13) where the RSC potential was used for curve 2 and the Paris potential was used for curve 4.

Comparison of the calculated spectral functions with experiment shows that there is good agreement for the range 50<q<250 MeV/c. Above 250 MeV/c the experimentally derived spectral function is substantially larger than theory. Below 50 MeV/c the data are about 50% smaller than theory. The discrepancy between data and theory at low q may be ascribed to the low relative energy between the ejected deuteron and the recoil proton for these ^{3}He(p,pd)p data points.

It is also noted that upon comparing the various calculated spectral functions to each other, they yield essentially identical results up to over 300 MeV/c in recoil momentum. Above 350 MeV/c they begin to show small deviations from each other, though a much larger deviation from experiment. It appears, then, that the calculated spectral functions are largely insensitive to calculational techniques or the choice of nucleon-nucleon potential.

In Fig. 4 the spectral function extracted from the present experiment is compared to that extracted from the ^{3}He(e,e´p)d experiment of Jans et al. (Ref. 14) at 530 MeV. Also shown is the spectrral function calculated by Ciofi degli Atti et al. (Ref. 9) as a representative comparison to theory. The agreement between the two experimental spectral functions is good only for 50<q<200 MeV/c. Above 200 MeV/c the (e,e´p) spectral function falls consistently below the (p,2p) and (p,pd)

results. This problem at large q is potentially interesting. One should note that the (e,e´p) results tend to follow theory up to about 300 MeV/c although a careful examination of Fig. 4 will show that the (e,e´p) results underestimate theory by about 50% for q>~100 MeV/c. This loss of experimental spectral function strength has been attributed by Laget (Ref. 15) to final state interaction effects. Recently data have been obtained at NIKHEF for the ^{3}He(e,e´p) reaction (Ref. 16) up to q ~500 MeV/c. The data for 0<q<250 Mev/c confirm the results of Jans et al. The higher recoil momentum data are not available at the present time.

Figure 5 shows a comparison of the present results with the spectral function of Ciofi degli Atti et al. which has been been multiplied by the factor $(1+q/285)^{2.5}$ and renormalized. The resulting distribution is almost identical to that obtained by Sick, Day and McCarthy (Ref. 17) who used the same factor to modify the spectral function of Dieperink et al. to give a good, empirical fit to their inclusive electron scattering data on ^{3}He. Curiously, this modified spectral function agrees fairly well with the results of the present experiment also.

Figure 6 shows, again, all the present results compared with additional calculations. Curve 1 is a PWIA calculation of the overlap integral of an Irving-Gunn ^{3}He wave function with a Hulthen deuteron wave function. Curves 2 and 3 are the spectral functions calculated by Gibson and Lehman (Ref. 18). Here, a separable nucleon-nucleon potential of the Yamaguchi form acting only in the $^1S_0$ and $^3S_1$ - $^3D_1$ states was used. The strength and

range parameters were determined by fitting the low energy properties of the nucleon-nucleon system such as scattering length, effective range, deuteron binding energy and quadrupole moment. Two different contributions of the D-state to the deuteron wave function were taken into account, 7% and 4% for curves 2 and 3, respectively. It is seen that none of these calculations fit the data in the high recoil momentum region. When compared to the spectral functions of Fig. 3, represented in Fig. 6 by the spectral function of Ciofi degli Atti et al. (curve 4) the Irving-Gunn and Gibson and Lehman spectral functions produce less strength at large q.

In an attempt to further understand the problems at large q a Distorted Wave Impulse Approximation DWIA calculation was performed using the code THREEDEE (Ref. 19). The optical model parameters used for this calculation were obtained from fits to p-d and p-^{3}He elastic scattering data. One should note that this type of calculation becomes increasingly less accurate and less appropriate as one considers very light nuclear systems. The results of this calculation are unclear since they tend to be similar to but not identical to the PWIA calculations described above. One might conclude from this that distortions may not play a large role in the reactions considered here. This is consistent with the fact that most of our experimental results agree well with the PWIA predictions in the low q region.

CONCLUSIONS

The results for the experimentally determined spectral function for ^{3}He obtained from the present (p,2p) and (p,pd) reaction studies can be summarized as follows. For $50<q<200$ MeV/c the data agree well with PWIA predictions using realistic three-nucleon wave functions. They also agree modestly well with the spectral function extracted from the ^{3}He(e,e´p)d data. Above q=200 MeV/c the (e,e´p) and theoretically determined spectral functions fall substantially below the (p,2p) and (p,pd) results with the discrepancy increasing with increasing q. A somewhat similar situation has been observed in the case of deuterium. However, one should note some important differences between the deuterium and ^{3}He cases. The momentum distribution of the deuteron was extracted from ^{2}H(p,2p)n data taken under various kinematic conditions. These momentum distributions do not agree well with each other in contrast to the situation for ^{3}He (Ref. 20). Moreover, some of the ^{2}H(p,2p)n data are kinematically in a region where intermediate delta production should play a large role and recent calculations by Yano (Ref. 21) confirm the importance of virtual delta production for these data. Most of the ^{3}He data shown here are kinematically well removed from the influence of intermediate delta production effects.

The ^{4}He(p,2p)^{3}H reaction has also been studied previously at intermediate energies (Ref. 21). The latter data were analyzed using the DWIA. Here, distortion effects are evident even at q=0. The DWIA provided a reasonably good fit to most of

the data using a wave function that was fit to the ^{4}He charge form factor extracted from elastic electron scattering data, after meson exchange current effects were removed. However, the data tend to lie above the DWIA predictions for q>200 MeV/c. It is unclear whether the inadequacy of the DWIA calculations indicates the influence of reaction mechanisms not accounted for by the calculations or whether part or all of the differences are due to lack of high momentum strength in the ^{4}He wavefunction used.

For the ^{3}He spectral function derived from the (p,2p) and (p,pd) reactions for q>200 MeV/c one is tempted to conclude that the differences between experiment and theory and with the (e,e'p) results are due to the increasing influence of reaction mechanisms other than given by the PWIA, and this may in fact be the case. However, following the discussion given above it is difficult to determine which reaction mechanism may be responsible for the large differences observed at large q values. It is possible that defects in the ^{3}He wavefunctions at large q may yet be responsible for some of these problems. In this regard one should note that recently Ishikawa et al. (Ref. 23) have shown that the inclusion of three-nucleon potentials in a Faddeev calculation for the triton yield a substantial improvement in the calculated triton binding energy. It would be very interesting to compare a spectral function obtained from similar calculations with our experimentally determined results.

REFERENCES

*Work supported in part by the National Science Foundation, USA and the Natural Sciences and Engineering Research Council of Canada.

+Present address: Dipartimento di Fisica, Universita di Milano, I20133 Milano, Italy.

++Present address: Sandoz AG, Pharma Department, CH 4002, Basel, Switzerland.

+++Present address: Rutherford Appleton Laboratory, Chilton, Didcot, Oxfordshire OX11 OQX, England.

++++Present address: Department of Physics, University of California, Irvine, CA 92717, USA

1. I. Slaus, M.B. Epstein, G. Paić, J.R. Richardson, D.L. Shannon, J.W. Verba, H.H. Forster, C.C. Kim, D.Y. Park and L.C. Welch, Phys. Rev. Lett. 27, 751 (1971); S.N. Bunker, M. Jain, C.A. Miller, J.M. Nelson and W.T.H. van Oers, Phys. Rev. C12, 1396 (1975); A.A. Cowley, P.G. Roos, H.G. Pugh, V.K.C. Cheng and R. Woody III, Nucl. Phys. A220, 429 (1974).

2. R. Frascaria, V. Comparat, N. Marty, M. Morlet, A. Willis and N. Willis, Nucl. Phys. A178, 307 (1971).

3. P. Kitching, G.A. Moss, W.C. Olsen, W.J. Roberts, J.C. Alder, W. Dollhopf, W.J. Kossler, C.F. Perdrisat, D.R. Lehman and J.R. Priest, Phys. Rev. C6, 769 (1972).

4. A. Bracco, H.P. Gubler, D.K. Hasell, W.P. Lee, W.T.H. van Oers, M.B. Epstein, D.A. Krause, D.J. Margaziotis, R. Abegg, C.A. Miller and A.W. Stetz, Phys. Lett. B137, 311 (1984).

5. D.K. Hasell, R. Abegg, B.T. Murdoch, W.T.H. van Oers, H. Postma and J. Soukup, Nucl. Instr. Methods 189, 341 (1981).

6. A. Bracco, H.P. Gubler, D.K. Hasell, W.T.H. van Oers, R. Abegg, C.A. Miller, M.B. Epstein, D.A. Krause, D.J. Margaziotis and A.W. Stetz, Nucl. Instr. Methods 219, 329 (1984).

7. Obtained from the phase shift analysis of R.A. Arndt, L.D. Roper, R.A. Bryan, R.B. Clark, B.J. VerWest and P. Signell through a computer interactive dial-in system (SAID).

8. O. Chamberlain and M.O. Stern, Phys. Rev. 94, 666 (1953); O. Chamberlain and D.D. Clark, Phys. Rev. 102, 473 (1956); H. Postma and R. Wilson, Phys. Rev. 121, 1229 (1961); K. Kuroda, A. Michalowicz and M. Poulet, Nucl. Phys. 88, 33 (1966); R.D. Schamberger, Phys. Rev. 85, 424 (1951); N.E. Booth, C. Dolnick, R.J. Esterling, J. Parry, J. Scheid and D. Sherden, Phys. Rev. D4, 1261 (1971); E.T. Boschitz, W.K. Roberts, J.S. Vincent, M. Blecher, K. Gotow, P.C. Gugelot, C.F. Perdrisat, L.W. Swenson and J.R. Priest, Phys. Rev. C6, 457 (1972); E. Winkelmann, P.R. Bevington, M.W. McNaughton, H.B. Willard, F.H. Cverna, E.P. Chamberlin, and N.S.P. King, Phys. Rev. C21, 2535 (1980).

9. C. Ciofi degli Atti, E. Pace and G. Salmé, in Proceedings of the Miniconference on the Study of Few-Body Systems with Electromagnetic Probes (Amsterdam, 1981), p.103

10. P. Nunberg, D. Prosperi and E. Pace, Nucl. Phys. A285, 58 (1977).

11. A.E.L. Dieperink, T. De Forest Jr., I. Sick and R.A. Brandenburg, Phys. Lett. 63B, 261 (1976).

12. R.A. Brandenburg, Y.E. Kim and A. Tubis, Phys. Rev. C12, 1368 (1975).

13. H. Meier-Hajduk, Ch. Hajduk, P.U. Sauer and W. Theis, Nucl. Phys. A395, 332 (1983).

14. E. Jans, P. Barreau, M. Bernheim, J.M. Finn, J. Morgenstern, J. Mougey, D. Tarnowski, S. Turck-Chieze, S. Frullani, F. Garibaldi, G.P. Capitani, E. de Sanctis, M.K. Brussel and I. Sick, Phys. Rev. Lett. 49, 974 (1982).

15. J.M. Laget, in Proceedings of the Third Miniconference on Coincident Reactions with Electromagnetic Probes, (Amsterdam 1983), p.149.

16. J.F.J. van den Brand, J.W.A. den Herder, E. Jans, A. Kaarsgaarn, P.H.M. Keizer, L. Lapikás, E.N.M. Quint, P.K.A. de Witt Huberts, H.P. Blok and G. van der Steenhoven, Contribution A25 to the Particles and Nuclei Tenth International Conference, Heidelberg, 1984; and private communication.

17. I. Sick, D. Day and J.S. McCarthy, Phys. Rev. Lett. 45, 871 (1980).

18. B.F. Gibson and D.R. Lehman, Phys. Rev. C29, 1017 (1984).

19. N.S. Chant, private communication.

20. C.F. Perdrisat, L.W. Swenson, P.C. Gugelot, E.T. Boschitz, W.K. Roberts, J.S. Vincent and J.R. Priest, Phys. Rev. 187, 1201 (1969); R.D. Felder, T.R. Witten, T.M. Williams, M. Furić, G.S. Mutchler, N.D. Gabitzsch, J. Hudomalj-Gabitzsch, J.M. Clement Jr., G.C. Phillips, E.V. Hungerford, L.Y. Lee, M. Warneke, B.W. Mayes and J.C. Allred, Nucl. Phys. A264, 397 (1976).

21. A. Yano, to be published.

22. W.T.H. van Oers, B.T. Murdoch, B.K.S. Koene, D.K. Hasell, R. Abegg, D.J. Margaziotis, M.B. Epstein, G.A. Moss, L.G. Greeniaus, J.M. Greben, J.M. Cameron, J.G. Rogers and A.W. Stetz, Phys. Rev. C25, 390 (1982).

23. S. Ishikawa, T. Sasakawa, T. Sawada and T. Ueda, Phys. Rev. Lett. 53, 1877 (1984).

FIGURE CAPTIONS

1. First order diagram for the ^{3}He(p,2p)d and ^{3}He(p,pd)p reactions. Particles 1-5 represent, in order, the incident proton, the target nucleus ^{3}He, the scattered proton, the ejected proton or deuteron and the recoiling particle.

2. A typical histogram of the missing energy for ^{3}He(p,pd)p. The events outside the peak region defined by the two arrows were rejected.

3. Experimental spectral functions (momentum distribution times the spectroscopic factor) as a function of the p-d relative momentum. Present measurements and previous ^{3}He(p,pd)p SREL results at 590 MeV. Curves 1-4 are PWIA calculations of Ciofi degli Atti et al. (1), Meier-Hajduk et al. (2 and 4), and Dieperink et al.(3) as described in the text.

4. Experimental spectral functions from the present measurements and from the ^{3}He(e,e'p)d Saclay results at 530 MeV. The curve is the spectral function of Ciofi degli Atti et al.

5. Experimental spectral function compared to the spectral function calculated by Ciofi degli Atti modified by the factor adopted from Ref. 17 as explained in the text.

6. The experimental spectral function from the present measurements compared to the spectral function calculated using an Irving-Gunn wavefunction (1) and the spectral functions

calculated by Gibson and Lehman (2 and 3) using 7% and 4% D-state in the deuteron, respectively. Curve 4 is the spectral function of Ciofi degli Atti et al.

TABLES

1. The ^{3}He(p,2p)d five-fold differential cross section results tabulated together with the quantities needed to deduce the spectral function in the framework of the PWIA. Θ_{cm} is the p-p scattering angle in the center of mass system of the scattered and ejected protons and T_{lab} is the corresponding laboratory energy.

2. The ^{3}He(p,pd)p five-fold differential cross section results tabulated together with the quantities needed to deduce the spectral function in the framework of the PWIA. Θ_{cm} is the p-d scattering angle in the center of mass system of the scattered proton and ejected deuteron and T_{lab} is the corresponding laboratory energy.

TABLE I

p_5 (MeV/c)	T_3 (MeV)	T^{p-p}_{lab} (MeV)	θ_{cm}	$(d\sigma/d\Omega)^{p-p}$ (mb/sr)	Kin. Factor (MeV/c^3 MeV^{-1})	$d^5\sigma/(d\Omega_3 d\Omega_4 dT_4)$ ($\mu b/sr^2$ MeV)
$^3He(p,2p)d$ $T_1 = 450$ MeV, $\theta_3 = 46^\circ$, $\theta_4 = 46^\circ$						
340	325	458	92.6°	3.60	$0.259 * 10^7$	1.26 ± 0.14
398	335	439	91.9°	3.67	$0.287 * 10^7$	0.954 ± 0.124
$^3He(p,2p)d$ $T_1 = 450$ MeV, $\theta_3 = 70^\circ$, $\theta_4 = 30^\circ$						
356	200	535	125.7°	3.81	$0.271 * 10^7$	1.24 ± 0.09
394	210	525	125.7°	3.81	$0.276 * 10^7$	0.857 ± 0.070
435	220	511	125.7°	3.79	$0.283 * 10^7$	0.738 ± 0.064
481	230	494	125.7°	3.78	$0.293 * 10^7$	0.482 ± 0.050
535	240	470	124.5°	3.78	$0.313 * 10^7$	0.333 ± 0.041
$^3He(p,2p)d$ $T_1 = 300$ MeV, $\theta_3 = 70^\circ$, $\theta_4 = 33^\circ$						
350	152	342	121.9°	3.86	$0.220 * 10^7$	1.53 ± 0.09
407	162	324	121.2°	3.80	$0.239 * 10^7$	1.17 ± 0.08

TABLE II

$^3He(p,pd)p$ $T_1 = 450$ MeV, $\theta_3 = 25^\circ$, $\theta_4 = 68^\circ$

p_5 (MeV/c)	T_4 (MeV)	T^{p-d}_{lab} (MeV)	θ_{cm}	$(d\sigma/d\Omega)^{p-d}$ ($\mu b/sr$)	Kin. factor (MeV/c^3 MeV^{-1})	$d^5\sigma/(d\Omega_3 d\Omega_4 dT_4)$ ($\mu b/(sr^2$ MeV))
5	50	442	40.8°	613 ± 57	$0.207 * 10^7$	460 ± 11
72	65	435	40.6°	624 ± 60	$0.240 * 10^7$	191 ± 5.0
116	75	428	40.5°	636 ± 62	$0.261 * 10^7$	58.1 ± 1.7
181	90	413	40.4°	661 ± 64	$0.292 * 10^7$	7.51 ± 0.36
225	100	399	40.4°	686 ± 82	$0.313 * 10^7$	2.91 ± 0.22
270	110	383	40.4°	730 ± 88	$0.337 * 10^7$	1.40 ± 0.15
294	115	374	40.4°	795 ± 95	$0.350 * 10^7$	1.26 ± 0.17
343	125	353	40.9°	902 ± 108	$0.380 * 10^7$	0.926 ± 0.139
398	135	327	41.5°	1050 ± 126	$0.424 * 10^7$	0.677 ± 0.119
465	145	291	42.6°	1178 ± 141	$0.514 * 10^7$	0.249 ± 0.080

$^3He(p,pd)p$ $T_1 = 450$ MeV, $\theta_3 = 50^\circ$, $\theta_4 = 68^\circ$

260	115	503	69.4°	747 ± 48	$0.370 * 10^7$	0.342 ± 0.086
264	125	501	69.0°	746 ± 48	$0.407 * 10^7$	0.217 ± 0.076
278	135	494	68.5°	745 ± 48	$0.452 * 10^7$	0.172 ± 0.070

^3He $(p,pd)p$ $T_1 = 450$ MeV, $\theta_3 = 70^\circ$, $\theta_4 = 30^\circ$

p_5 (MeV/c)	T_3 (MeV)	T^{p-d}_{lab} (MeV)	θ_{cm}	$(d\sigma/d\Omega)^{p-d}$ (nb/sr)	Kin. factor (MeV/c^3 MeV^{-1}	$d^5\sigma/d\Omega_3 d\Omega_4 dT_3$ ($\mu b/sr^2$MeV)
126	200	401	110.1°	36.9 ± 4.8	$0.327 * 10^7$	5.23 ± 0.18
153	210	404	110.3°	36.6 ± 3.7	$0.356 * 10^7$	3.04 ± 0.14
187	220	404	110.5°	36.6 ± 3.7	$0.397 * 10^7$	1.70 ± 0.10
229	230	402	110.4°	36.8 ± 4.0	$0.463 * 10^7$	0.876 ± 0.071
287	240	394	110.1°	37.6 ± 5.3	$0.624 * 10^7$	0.523 ± 0.053

$^3He(p,pd)p$ $T_1 = 300$ MeV, $\theta_3 = 70^\circ$, $\theta_4 = 33^\circ$

83	140	276	106.4°	64.1 ± 10	$0.263 * 10^7$	20.8 ± 0.34
121	150	278	106.6°	63.3 ± 10	$0.301 * 10^7$	11.6 ± 0.25
173	160	276	106.5°	64.0 ± 10	$0.377 * 10^7$	5.17 ± 0.17

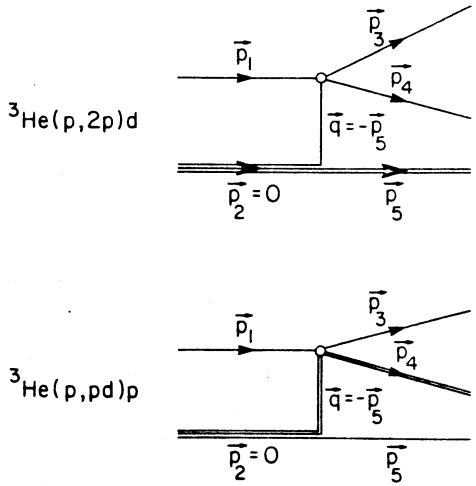

Fig. 1

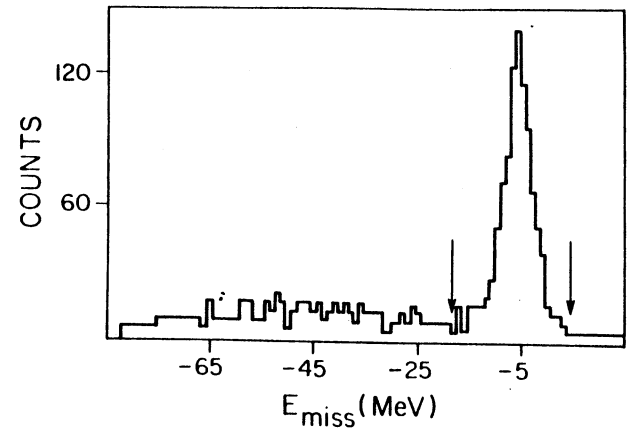

Fig. 2

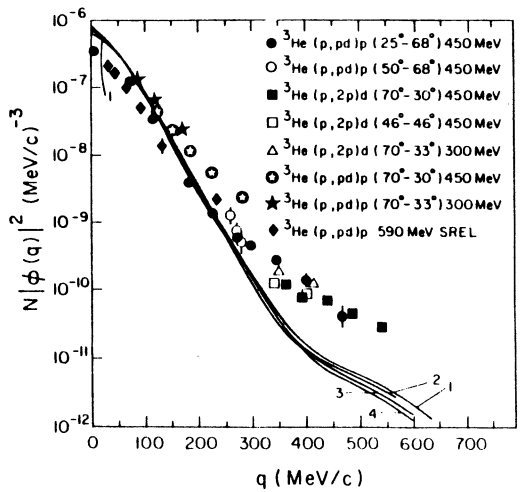

Fig. 3

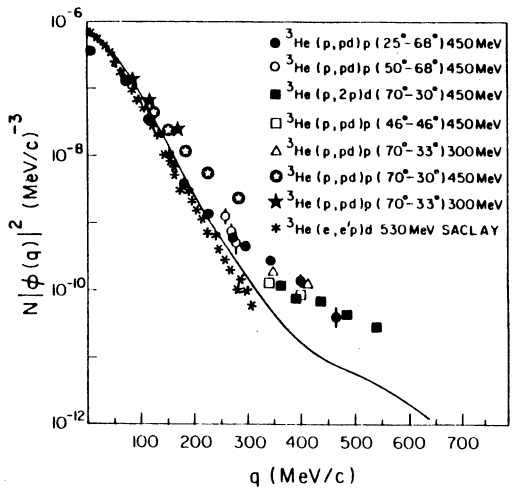

Fig. 4

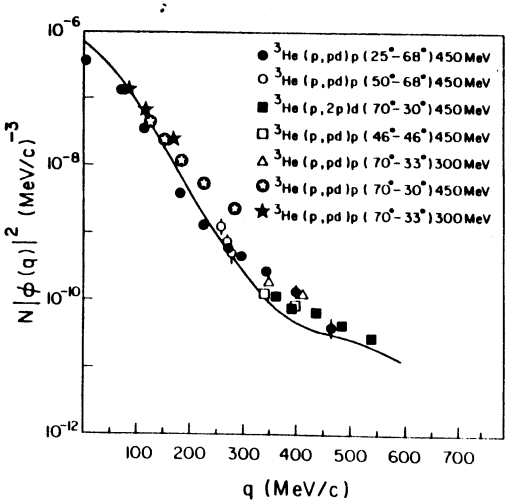
10^{-6}
10^{-8}
10^{-10}
10^{-12}
$N|\phi(q)|^2$ (MeV/c)$^{-3}$
100 200 300 400 500 600 700
q (MeV/c)
● ^{3}He (p,pd)p (25°-68°) 450 MeV
○ ^{3}He (p,pd)p (50°-68°) 450 MeV
■ ^{3}He (p,2p)d (70°-30°) 450 MeV
□ ^{3}He (p,pd)p (46°-46°) 450 MeV
△ ^{3}He (p,pd)p (70°-33°) 300 MeV
⊙ ^{3}He (p,pd)p (70°-30°) 450 MeV
★ ^{3}He (p,pd)p (70°-33°) 300 MeV

Fig. 5

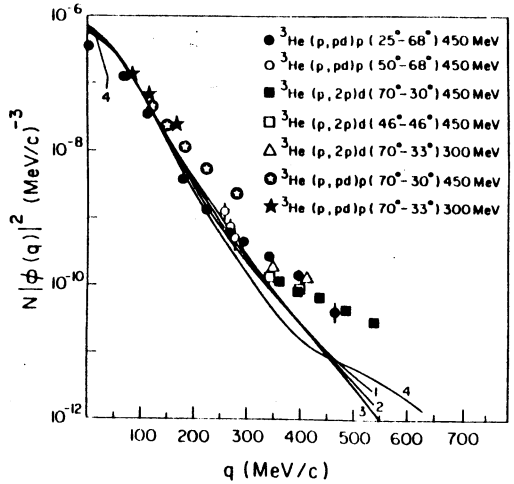
10^{-6}
10^{-8}
10^{-10}
10^{-12}
$N|\phi(q)|^2$ (MeV/c)$^{-3}$
100 200 300 400 500 600 700
q (MeV/c)
● ^{3}He (p,pd)p (25°-68°) 450 MeV
○ ^{3}He (p,pd)p (50°-68°) 450 MeV
■ ^{3}He (p,2p)d (70°-30°) 450 MeV
□ ^{3}He (p,2p)d (46°-46°) 450 MeV
△ ^{3}He (p,2p)d (70°-33°) 300 MeV
⊙ ^{3}He (p,pd)p (70°-30°) 450 MeV
★ ^{3}He (p,pd)p (70°-33°) 300 MeV
4
4
1
2
3

Fig. 6